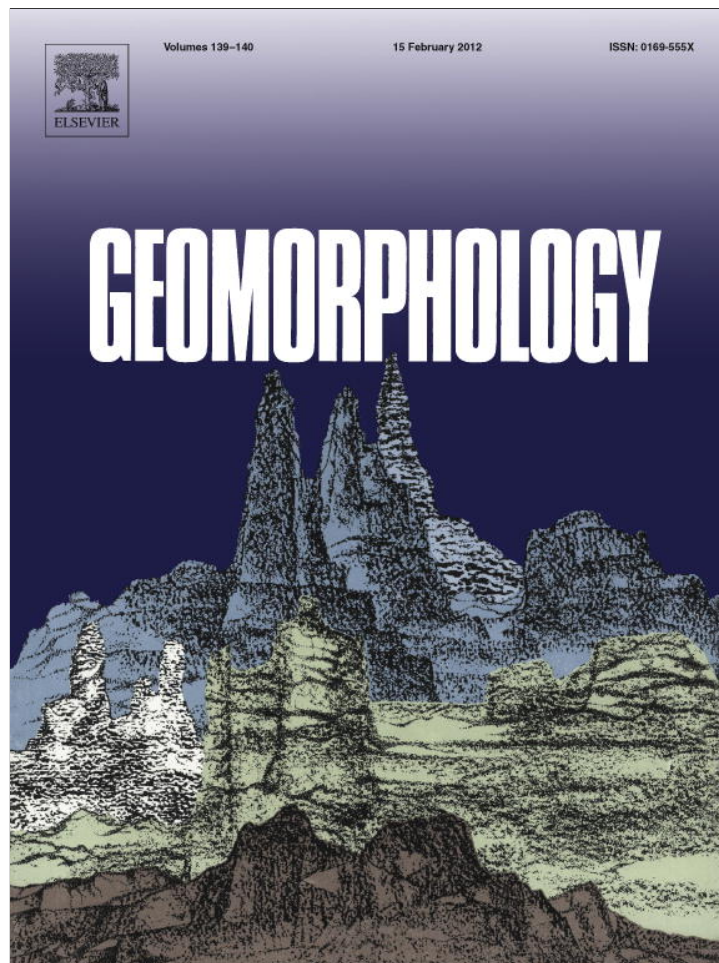


Provided for non-commercial research and education use.
Not for reproduction, distribution or commercial use.



This article appeared in a journal published by Elsevier. The attached copy is furnished to the author for internal non-commercial research and education use, including for instruction at the authors institution and sharing with colleagues.

Other uses, including reproduction and distribution, or selling or licensing copies, or posting to personal, institutional or third party websites are prohibited.

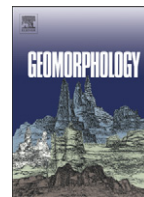
In most cases authors are permitted to post their version of the article (e.g. in Word or Tex form) to their personal website or institutional repository. Authors requiring further information regarding Elsevier's archiving and manuscript policies are encouraged to visit:

<http://www.elsevier.com/copyright>



Contents lists available at SciVerse ScienceDirect

Geomorphology

journal homepage: www.elsevier.com/locate/geomorph

Geomorphic process rates of landslides along a humidity gradient in the tropical Andes

J. Muenchow^{a,*}, A. Brenning^b, M. Richter^a^a Institute of Geography, University of Erlangen-Nuremberg, Kochstr. 4, 91054 Erlangen, Germany^b Department of Geography and Environmental Management, University of Waterloo, 200 University Avenue West, Waterloo, Ontario N2L 3G1, Canada

ARTICLE INFO

Article history:

Received 22 April 2010

Received in revised form 7 September 2011

Accepted 30 October 2011

Available online 4 November 2011

Keywords:

Mass movements

Denudation rate

Geomorphic work

Generalized additive model

ABSTRACT

Areas with high landslide activity and diversity were encountered in the tropical Andes of Southern Ecuador under contrasting, semi-arid to perhumid climatic conditions. The objective of this study was to determine and compare geomorphic process rates of shallow landslides along this remarkable humidity gradient and subject to different types of human-made and natural environmental changes. Geomorphic work, geomorphic power and landslide mobilization rate (*LMR*) were therefore calculated for shallow landslides in two study areas with two separate geological or land use-related subareas each. While landslide ages were known in the perhumid Reserva Biológica San Francisco (RBSF) area, only an approximation of the frequency of critical landslide-triggering rainfall events was available for the semi-arid Masamanaca area. Landslide volumes were estimated by volume–area scaling. Generalized additive models (GAMs) were used as landslide susceptibility models in order to analyze the relative importance of topography, and to downscale *LMR* values to a fine spatial resolution. *LMR* in the perhumid RBSF area ranged from $\approx 2 \text{ mm yr}^{-1}$ in the natural part of this area with tropical mountain rainforests to $\approx 5 \text{ mm yr}^{-1}$ in the human-influenced part. The semi-arid Masamanaca area, though subject to greater estimation uncertainties, displayed *LMR* on the order of ≈ 0.4 to 4 mm yr^{-1} for shallow landslides. The results provide a basis for the spatially differentiated assessment of landscape evolution and degradation in an area with a close relation between landslide activity, natural vegetation succession and human land use.

© 2011 Elsevier B.V. All rights reserved.

1. Introduction

Landslides are common phenomena in the Andes of Southern Ecuador, where they not only cause economic damage, but also enhance biodiversity and contribute to landscape evolution in a megadiverse hotspot (>5000 vascular plant species per $10,000 \text{ km}^2$; Barthlott et al., 2007) that is currently the focus of a large coordinated research cluster of the German Science Foundation (e.g., Beck et al., 2008a; Richter, 2009). This study investigated geomorphic process rates along a remarkable climatic gradient that is characterized by a precipitation difference of up to several thousand mm (Figs. 1 and 2). The region thus constitutes an excellent laboratory for investigating relationships among climate, vegetation, and geomorphic processes in complex terrain, as humid areas with tropical mountain rainforests on the eastern slope of the Cordillera and semi-arid pastureland in the Interandean Sierra in the west occur within 20 km of distance from each other. Although the general importance of landslides in the Cordillera Real of Southern Ecuador is known (Hagedorn, 2002;

Lozano et al., 2005), research has been limited to the mountain rainforest areas (Stoyan, 2000; Wilcke et al., 2003; Busmann et al., 2008; Restrepo et al., 2009).

For the purpose of comparing process rates of the semi-arid and perhumid slopes of the tropical Andes (Emck, 2007; Beck et al., 2008b), we estimated denudation rates (Crozier, 1984) and geomorphic work (Caine, 1976) and determined site conditions that control the susceptibility to landslide initiation based on empirical generalized additive models. In this context we present a novel application of these models for downscaling the spatial distribution of geomorphic process rates within the study areas. While data for both shallow and deep-seated mass movements were collected and described, our main focus was on shallow mass movements that were classified as being triggered by rainfall events. This subset was chosen because the governing hydrometeorological and geomorphological processes are more homogeneous for these features, which allowed us to apply volume–area scaling methods, assess the frequency of landslide-triggering events, and ultimately calculate and downscale geomorphic process rates. We discuss the results and uncertainties in terms of their implications for landscape evolution and regarding linkages between ecological and geomorphic processes as well as future research needs.

* Corresponding author. Tel.: +49 9131 8522921.

E-mail address: jannes.muenchow@geographie.uni-erlangen.de (J. Muenchow).

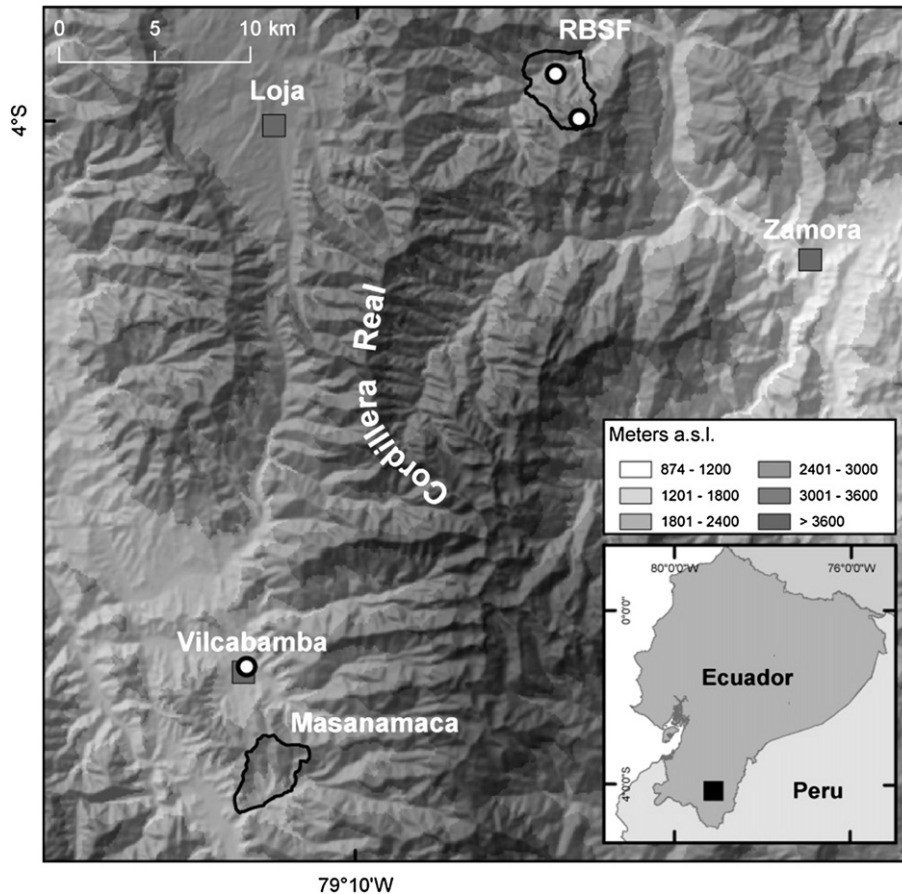


Fig. 1. Location map of the study areas: Reserva Biológica San Francisco (RBSF) and Masanamaca. White dots represent weather stations.

2. Study areas

We investigated landslide distribution and geomorphic process rates in two study areas, the Reserva Biológica San Francisco (RBSF) and the Masanamaca area, which are located in the Andes of Southern Ecuador on the semi-arid and perhumid sides of the continental divide within a distance of about 35 km (Fig. 1). The most striking

difference between the study areas is related to the significant humidity gradient across the Cordillera Real, which additionally varies between El Niño Southern Oscillation (ENSO) episodes (Emck, 2007; Rossel and Cadier, 2009). The eastern slope of the Cordillera Real is subject to nearly daily rainfall brought by continent-crossing trade winds from the Atlantic. Therefore the annual precipitation values in the RBSF ranged from 2000 mm in the lower parts to more

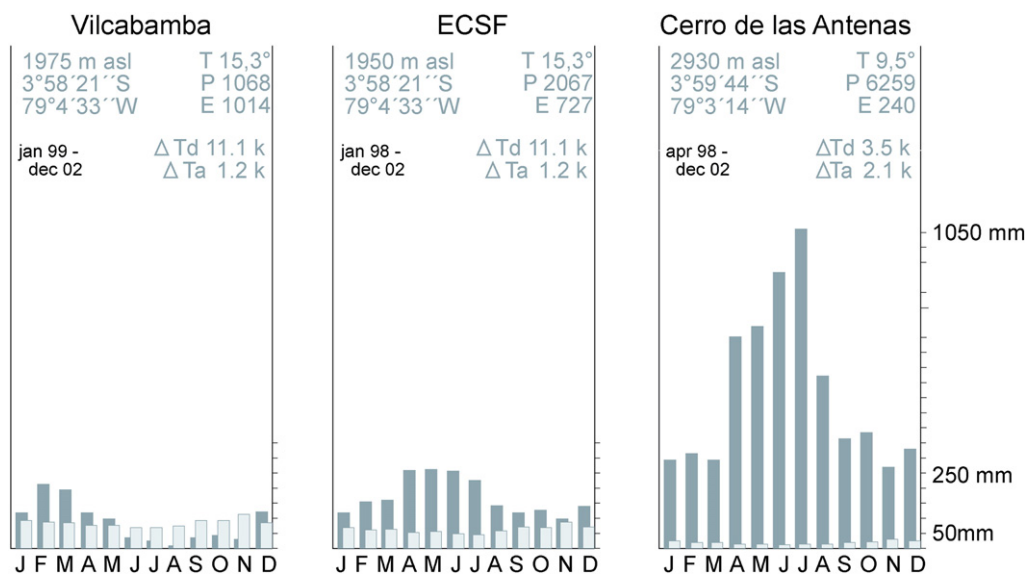


Fig. 2. Climate diagrams for both slopes of the Cordillera Real. Locations of the climate stations can be viewed in Fig. 1. ECSF and Cerro de las Antenas belong to the RBSF study area. Modified after Emck (2007).

than 6000 mm in elevations between 2900 and 3100 m a.s.l. (Fig. 2; Emck, 2007). Hourly rainfall greater than 75 mm occurred especially in these upper parts, and such events were observed three times during a 9-year measurement period (1998–2007; Emck, 2007). The area is mostly underlain by metasiltstones, sandstones and quartzites. Interspersing layers of highly weathered phyllites and clay schists are present, and may favor landslide activity (Litherland et al., 1994; Beck et al., 2008b). The steep slopes of the study area are covered with evergreen lower and upper mountain rainforest. Only the area north of the road (Fig. 3b) has been influenced ever since its construction in the 1960s by human activity in the form of cattle grazing (Stoyan, 2000; Peters et al., 2010).

The Masanamaca area as part of the inner-Andean basin lies in the rain shadow of the Cordillera Real (Fig. 1) and receives 700–1200 mm rainfall according to nearby observations in the north of Vilcabamba (Fig. 1; Emck, 2007). The maximum hourly rainfall amounted to 33 mm during a 5-year measuring period (1998–2003; Emck, 2007). The prevailing geological units consist of Tertiary continental sediments (mainly conglomerates, but also sand- and siltstones). Where exposed, surfaces are subject to a rapid dissection and badland development, which is at least partly due to the transformation of the natural vegetation (deciduous dry forest and shrub land) into pastureland; generally, badland development is widespread in this region (Vanacker et al., 2007a). Human-induced burning of vegetation occurs in regular intervals, to our knowledge roughly every four to seven years. Human activity dates back at least to the Inca Empire, as is visible from fortress remnants close to Vilcabamba. Prior to the Inca conquest in the 7th century, the climatically favored inner-Andean basins, especially Malacatos and Vilcabamba, were populated by different subgroups of the Paltas (Guffroy, 2006).

Both study areas are subject to regular earthquake occurrences as they form part of the circum-Pacific subduction zone. The first author witnessed two earthquakes in 2007 (9/25/2007, MW 5.9, ~250 km to the NE of the study areas; IGEPN, 2011; 11/16/2007, M 6.8, ~85 km to the NW of the study areas; USGS, 2011), but to the best of our knowledge and according to the first author's field observations, no new landslides occurred during these events. Ten earthquakes of MW 6.0 or greater occurred between 1990 and 2011 within up to ≈ 900 km from the study areas (IGEPN, 2011, information prior to 1990 not available). However, none of the earthquakes with magnitudes

above six occurred within less than 190 km of distance (with exception of the previously mentioned 11/16/2007 earthquake).

For modeling and the calculation of geomorphic process rates both study areas were further subdivided. The RBSF area was split according to land use resulting in a smaller human-influenced, northern part and a larger natural, southern part (Fig. 3). The Masanamaca area was divided according to the underlying geology in an eastern metamorphic and a western sedimentary part (Fig. 3).

3. Data and methods

3.1. Data

Landslides were mapped in the RBSF area in 1998 in the field by Stoyan (2000), who additionally used aerial photos of 1962, 1969, 1976, 1989, and 1998 (Instituto Geográfico Militar de Ecuador, IGM; scale 1:60,000). The first author additionally mapped landslides in this area from aerial photos of the years 1962 (IGM; scale 1:60,000) and 2000 (data source: E. Jordan and L. Ungerechts, Düsseldorf; scale 1:5000). He created the landslide inventory of the Masanamaca area during field work in 2007/08; each landslide was visited in the field. We consider both landslide inventories to be substantially complete, but it is possible that very small landslide scars (<100 m²) were undetected. However, their contribution to the geomorphic process rates would only be marginal. Mass movements were classified by the processes and materials involved following the scheme proposed by Dikau et al. (1996). Both shallow and deep-seated landslides were mapped. Yet only shallow landslides that were classified as rainfall-triggered were considered in the modeling and the calculation of geomorphic process rates. Throughout the text, shallow landslides refer to planar earth or debris slides; earth or debris flows; and complex movements such as earth or debris slide-flows (Wieczorek, 1987; Aleotti, 2004; Giannecchini, 2006). The collected landslide attributes included their activity (state, distribution and style of activity), their classification according to causative factors (preparatory, triggering and controlling factors) and underlying geology (Crozier, 1986; Cruden and Varnes, 1996). While landslide initiation is in most cases polycasual (Crozier, 1986; Dikau et al., 1996), we classified them according to what was judged to be the main preparatory, triggering and controlling factor, respectively, if possible.

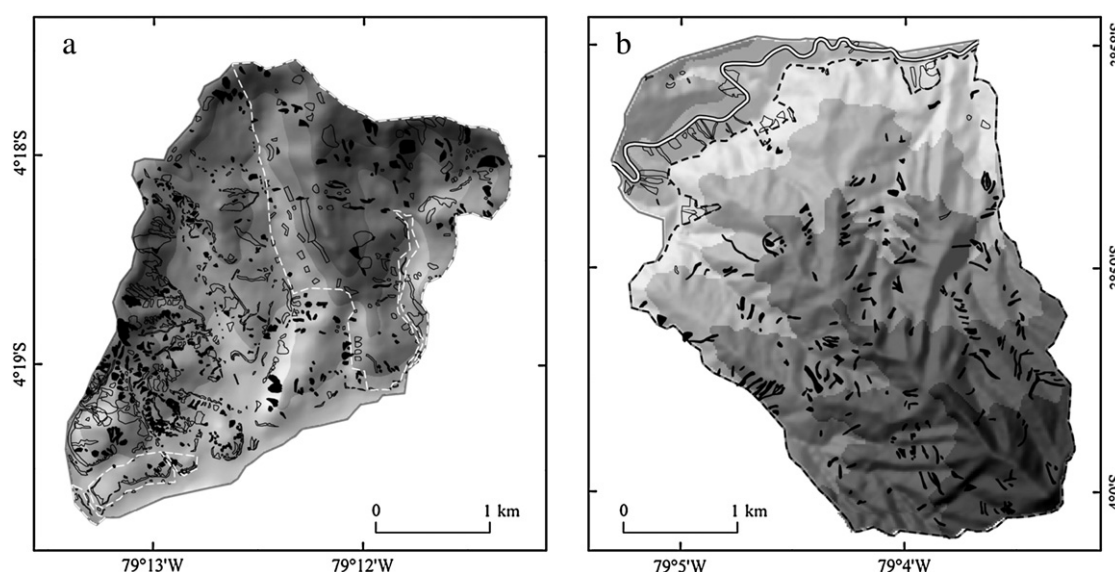


Fig. 3. Landslide distribution in the study areas of (a) Masanamaca and (b) RBSF. In (a), dashed white lines show areas with metamorphic rock. Filled polygons refer to shallow landslides triggered by intense rain events, which were used for modeling. In (b), landslides in 1998 after Stoyan (2000) are shown. Area surrounded by the dashed black line is covered with natural vegetation. Filled polygons refer to naturally and unfilled polygons to human-induced landslides. Both were used in the modeling. The white line with black outline in the northern part represents a road.

The digital elevation model (DEM) available for mapping and modeling in the Masamanaca area was photogrammetrically derived and has a 10 × 10 m resolution (data source: E. Jordan and L. Ungerechts, Düsseldorf). However, steep west-exposed slopes in the metamorphic area were not accurately represented in this DEM because of cast shadow in the aerial photos. In the RBSF area, Stoyan (2000) provided a 10 × 10 m resolution DEM based on stereoscopic aerial photo analysis. A higher-quality photogrammetric DEM was also available for this area (original resolution 1 × 1 m, resampled to 10 × 10 m, based on aerial photos of the year 2000; data source: E. Jordan and L. Ungerechts, Düsseldorf), but could not be used in conjunction with the earlier inventories because of small geometric distortions of the older data. The influence of mass movements on the DEM's surface topography is negligible given its limited level of detail. DEM-derived slope angles had a maximum of 66° in the Masamanaca area and of 88° in the higher-quality, but slightly noisier photogrammetric DEM of the RBSF area, whereas the maximum was at 64° for Stoyan's less accurate and smoother DEM. Table 1 shows additional descriptive summary data of terrain attributes.

3.2. Methods

3.2.1. Estimation of geomorphic process rates

We calculated geomorphic process rates to assess the contribution of shallow landslides to landscape evolution (Caine, 1976). Process rates were estimated in the first place as average values of each study area and time period represented, and were later downscaled to the DEM resolution based on empirical models of landslide initiation (see Section 3.2.3).

Specifically, we determined the landslide mobilization rate (*LMR*) in the sense of a lowering rate vertical to the surface (Guzzetti et al., 2009) and the geomorphic work as key geomorphic process rates. Landslide volumes, the recurrence interval of landslide-triggering events, and the density of the scoured material were intermediate variables that needed to be estimated. In the Masamanaca area, *LMR* was only calculated for shallow landslides, because estimates of recurrence intervals could only be calculated for rainfall as their trigger, but not for deep-seated ones. In the RBSF area, in contrast, only shallow landslides were observed, and landslide-generating periods were known from multitemporal aerial photos. Other denudation processes were present in both study areas (Sections 3.1 and 4.1) but were not included in the calculated *LMR* values.

LMR (mm yr⁻¹) can be calculated after Crozier (1984) as

$$LMR = (V_{all}/A_t)/T \times 10^3 \quad (1)$$

where V_{all} is the volume of all considered landslides (m³), A_t is the “true” surface area of the study area (m²), and T is the time span

(yr) during which the landslides occurred. The “true” surface area corresponds to the three-dimensional (3D) area, and was computed using the area and volume statistics of the 3D Analyst Tool provided in ArcGIS 9.3. T may be expressed either as the time between two inventories used for identifying fresh landslides, or the time required for generating the observed population of shallow landslides, which depends on the critical-rainfall recurrence interval, as discussed later in this section. Volume–area scaling was used to estimate the volumes of all shallow landslides except those of the flow-type, for which a geometric approach was chosen. It is important to note that Eq. (1) only requires an estimate of the total landslide volume, which is less affected by uncertainties than estimates of individual landslide volumes.

In contrast to the denudation rate, which would be calculated only based on material that is removed from the study area, any material that is mobilized by landslides is included in the calculation of *LMR*, regardless of whether it is temporarily or permanently deposited within the study area itself (Guzzetti et al., 2009).

Since field measurements of landslide thicknesses are only available for eight landslides in the RBSF area, we used volume–area scaling and geometrical considerations to estimate the volume displaced by different types of landslides. The equation of Larsen et al. (2010) was used in this study, as it has been calibrated to a global landslide data set, and to our knowledge no specific volume–area scaling rule for shallow movements in the Andean region is available:

$$V = 0.644A^{1.145} \quad (2)$$

where V (m³) is the volume of a single landslide and A (m²) is the corresponding landslide area calculated from digitized landslide boundaries and DEMs. Uncertainties resulting from the reported standard errors of the two parameters of the power-law relationship are approximately ± 11% of the total landslide volume. A comparison of total volumes estimated with different scaling rules from different regional inventories suggested that the uncertainty related to local geological or climatic conditions may be of the order of factor 2 (six shallow-landslide scaling rules estimated from sample sizes > 100; Larsen et al., 2010).

For flow movements we used a simple geometric approach to estimate the volume based on a simple triangular model of channel geometry with channel sides inclined at the friction angle φ relative to the horizontal plane. The scoured maximum depth d perpendicular to the horizontal plane can then be calculated from the channel width as

$$d = \tan(\varphi)w/2. \quad (3)$$

Widths were estimated at the center of each flow, and we used a friction angle $\varphi = 30^\circ$ for all areas built up by metamorphic rock in

Table 1
Descriptive statistics (median and, in parentheses, interquartile range) of predictor variables in each subarea for landslide-initiation and non-landslide points.

| | Median (IQR) for landslide/non-landslide points | | | | | |
|------------------------------|---|-------------------|--|---|---|---|
| | Elevation (m) | Slope (°) | Plan curvature (10 ⁻³ m ⁻¹) | Profile curvature (10 ⁻³ m ⁻¹) | Log ₁₀ -Catchment area (m ²) | Log ₁₀ -Distance to road (m) |
| Masanamaca conglomerate | 1841 (165) / 1832 (176) | 29 (12) / 24 (13) | 3.88 (15.50) / 0.04 (13.86) | 5.25 (15.86) / -0.94 (9.63) | 2.60 (0.53) / 2.95 (0.72) | * |
| Masanamaca metamorphic | 2050 (283) / 2013 (205) | 31 (15) / 29 (14) | 0.60 (14.79) / -0.50 (10.35) | 3.70 (12.89) / 0.33 (10.29) | 2.92 (0.61) / 3.12 (0.64) | * |
| RBSF natural | 2348 (298) / 2297 (436) | 35 (16) / 32 (15) | 1.82 (13.43) / 1.20 (14.51) | 2.84 (16.61) / 0.82 (15.11) | 2.80 (0.41) / 2.90 (0.58) | 3.29 (0.27) / 3.23 (0.46) |
| RBSF human-influenced | 1894 (92) / 1920 (184) | 30 (16) / 31 (15) | 1.18 (7.37) / 0.49 (9.60) | 2.75 (12.66) / 0.76 (13.58) | 3.13 (0.59) / 2.99 (0.58) | 1.57 (1.22) / 2.06 (0.63) |
| RBSF natural (2000) | 2376 (155) / 2328 (428) | 45 (10) / 37 (15) | -22.63 (45.23) / 4.11 (30.51) | -7.63 (32.01) / 3.29 (29.62) | 2.40 (0.43) / 2.38 (0.61) | * |
| RBSF human-influenced (2000) | 1907 (102) / 1927 (165) | 43 (9) / 38 (15) | 0.49 (39.79) / 1.82 (29.46) | 8.86 (41.55) 0.31 (32.63) | 2.56 (0.65) / 2.58 (0.61) | * |

concordance with Riemer et al. (1989). Laboratory tests from these authors produced an effective friction angle between 26.5° and 30° for an area with metamorphic rocks north of our study area (Paute basin, Azuay). In the conglomerate area, a friction angle of 29° was assumed, which appears to be a plausible estimate for mixed soils underlain by conglomerates (see e.g., Prinz and Strauß, 2006), and was partly supported by the median slope angle of landslide initiation points (Table 1) and by parameter optimization within a physically-based SHALSTAB model (not shown). The calculated depths varied by $\pm 12\%$ under a $\pm 3^\circ$ deviation from the assumed friction angle.

Simplifying the shape of the flow movement including its channel to an isosceles triangular prism allowed calculating the volume from its width w , depth d and planimetric length l as

$$V_{\text{flow}} = 0.5wdl. \quad (4)$$

Depending on the mentioned thickness uncertainty for flow-type movements, their contribution to the total shallow landslide volume was of the order of 31–37% in the RBSF area and 0.9–1.1% in the Masanamaca area. Estimated total landslide volume was therefore relatively insensitive to thickness uncertainties related to uncertain friction angles, particularly in the Masamanaca area where only 16% of all movements were of the flow type, and because of the small area they contributed.

The time span T over which landslides occurred is known in the RBSF area because of the availability of time-lapse aerial photos. In the Masamanaca area, by contrast, the calculation of LMR was based on rather loose upper (100 years) and lower bounds (10 years) for T (the derivation of T is explained in more detail in the following paragraph) that account for the uncertainties in the estimation of a recurrence interval for critical rainfall events that likely triggered landslides, as well as the uncertainty regarding the number of such rainfall events that would be required to create the observed landslide population. This procedure only provided upper and lower bounds of the LMR in the Masamanaca area rather than a point estimate as in the RBSF area.

We derived the recurrence interval of the entire population of rainfall-induced landslides from estimated critical rainfall intensities and a 5-year time series of hourly precipitation data from Vilcabamba (1950 m a.s.l., February 1998 to March 2003; Emck, 2007; Fig. 1). Our focus was on empirical relationships developed in regions with similar topography and climate as in the Masamanaca area. Some empirical approaches would have resulted in unrealistically low critical rainfall intensities for the initiation of shallow sliding, which in turn would imply unrealistically short recurrence intervals of such triggering rain events on the order of less than a year (e.g., Caine, 1980; Wiczorek, 1987; Crosta and Frattini, 2001; Guzzetti et al., 2008); these estimates were therefore discarded. Alternative estimates of critical rainfall intensity for events of 1 to 38 h duration were calculated using several global (Jibson, 1989) and regional empirical relationships (Moser and Hohensinn, 1983; Cancelli and Nova, 1985; Aleotti, 2004; Giannecchini, 2006; Kanji et al., 2008). These estimates were derived by counting how often the gauged rainfall intensities exceeded the precipitation amounts proposed by the empirical relationships during the measuring period, giving us a recurrence interval for triggering rainfall events. However, we had to take into account (i) the short observation period of weather data, (ii) the unlikelihood that only one event created the observed shallow landslide inventory, and (iii) that the empirical thresholds were not explicitly produced for our study area. Accordingly, we decided to represent the time needed for regenerating the observed shallow landslides by a rather broad time span (10 to 100 years) based on the empirical relationships. Careful discussion of the calculated landslide process rates using the estimated time span was therefore required (see Sections 2 and 5.2).

The potential energy freed by landslide-induced erosion provides an alternative measure to the LMR. This is referred to as the geomorphic work and expressed as

$$\Delta E = V\rho h g/A_t \quad (5)$$

where ΔE is the potential work (in J km^{-2}), ρ represents the dry density of the displaced material (in kg m^{-3} , see below), h is the vertical displacement (in m) as defined below, g is the gravitational acceleration (9.81 m s^{-2}), and A_t is the area over which the work is observed (modified after Caine, 1976). It is alternatively expressed as a power $\Delta E/T$ (in W km^{-2}). We estimated the vertical difference h by measuring the elevation difference between the initiation point and the tip of the movement (Cruden and Varnes, 1996) in the DEM and subtracting one-third in order to adjust for the location of the center of mass before and after the displacement. This modification was reasonable as it can be assumed that the center of mass of the displaced mass neither slid through the upper nor the lower sixth of the actual landslide length. V is calculated as described above.

For soils underlain by conglomerates in the Masamanaca area, we assumed a dry bulk density of 1.3 g cm^{-3} based on field measurements by Hagedorn (2001) and Schubert (1999), which is consistent with measurements in a nearby area with similar geology and soil conditions (Molina et al., 2008; 1.35 g cm^{-3} average dry soil density). In the metamorphic RBSF area, field measurements indicate an average dry bulk density of 1.4 g cm^{-3} (Haubrich et al., submitted; Haubrich, personal communication, 2009); we assume the same value for the metamorphic part of the Masamanaca area.

3.2.2. Statistical modeling

Statistical-empirical landslide distribution models are widely used for landslide susceptibility mapping based on inventory data (Brenning, 2005). We used the generalized additive model (GAM) to analyze the distribution of landslide initiation points in each of the four study areas (Brenning, 2008), and to derive spatial patterns of LMR as a function of terrain attributes, as explained below. Displaying the LMR spatially represents the linkage between the modeling approach and the determination of the geomorphic process rates.

The statistical models were applied separately to each of the four subareas. For training the models, we used the initiation points of shallow mass movements and, as non-occurrence data, points outside the landslide polygons. Initiation points were digitized manually at the center of the landslide head scarps. In the natural RBSF area, models were created for the newer higher-quality data of the year 2000 as well as for the older data representing a longer time series.

The GAM is a flexible, yet interpretable model. It is a semiparametric extension of logistic regression that is able to include both linear and nonlinear influences of predictor variables on the response (Hastie, 2009). Nonlinear effects are represented by nonparametric smoothers as variable transformations. The additive model structure and the possible combination with linear predictors allow a simpler model visualization and interpretation than in, e.g., artificial neural networks or tree-based ensemble techniques. The GAM has also shown promising predictive performances in geomorphological distribution modeling in complex terrain (Brenning, 2008, 2009; Park and Chi, 2008; Goetz et al., 2011). We applied the GAM with landslide initiation points as the binary (presence/absence) response variable, and the following predictor variables:

- Local slope angle ($^\circ$) as a control of downslope shear stress.
- Log catchment area ($\log \text{ m}^2$), i.e. the decadic logarithm of the local topographic contributing area, representing the amount of water potentially flowing towards a location.
- Plan curvature (rad m^{-1}) expressing the degree of divergence or convergence of water flow as well as the exposure to wind.

- profile curvature (rad m^{-1}) or downslope change in slope angle as a measure of flow acceleration and exposure to wind.
- Log distance to road (log m) in the human-influenced part of the RBSF area as a proxy of the influence of debutting on slope hydrology and stability.
- Elevation (m a.s.l.) representing the altitudinal differentiation of vegetation and precipitation in the natural rainforest zone of the RBSF area.

For better comparison between the study areas, we did not perform a variable selection of the predictor variables. Only the representation of predictor variables as untransformed linear predictors or as transformed nonlinear predictors was controlled by stepwise variable selection. Model construction started with linear predictors and subsequently replaced them with nonlinear ones based on a stepwise forward and backward variable selection using the Akaike Information Criterion (AIC). AIC measures the statistical goodness of fit by penalizing for model size or complexity, in this case a linear versus a nonlinear representation of a variable. The lowest AIC value indicates the preferred model. The training set in each study area consisted of all landslide initiation points and the same number of randomly selected grid cells lying outside the boundaries of the observed landslides.

We assessed the relative variable importance in each model in terms of the deviance increase that results from dropping one variable at a time. The models' goodness of fit was expressed by the area under the receiver operating characteristic (ROC) curve (AUROC), which is a value between 0.5 (no discrimination of the two classes) and 1.0 (perfect discrimination). Since AUROC values that are estimated on the training set are overoptimistic, we also performed cross-validation for AUROC estimation. In cross-validation, a data set is randomly partitioned into k subsets (here: $k=5$), using one partition at a time as a test set, and the others as training sets, yielding a bias-reduced assessment of the predictive performance (Efron and Gong, 1983). This procedure is repeated 100 times in order to obtain estimates that are independent of a particular partitioning. This is referred to as (non-spatial) 100-repeated 5-fold cross-validation. Since spatially distributed samples are usually not statistically independent (Brenning, 2005; Atkinson and Massari, 2011), we furthermore used a spatial cross-validation in which the $k=5$ partitions were obtained by k -means clustering of sample coordinates (Ruß and Brenning, 2010).

All analyses were conducted in the software R using its packages 'gam' (Hastie, 2009) for statistical modeling and 'RSAGA' for geoprocessing with SAGA GIS (Brenning, 2008).

3.2.3. Downscaling of process rates

We used the predicted spatial probabilities of landslide initiation to downscale the average LMR obtained for each study area. Assuming that the landslide volume is independent of the probability of landslide occurrence $p(x)$ at a given location x , the local LMR at that location, $LMR(x)$, will be proportional to $p(x)$:

$$LMR(x) = qp(x) \tag{6}$$

where q is a parameter that depends on average LMR for the study area. Substituting this equation into the equation for average LMR over all grid cells,

$$LMR = (1/N) \sum_{i=1}^N LMR(x_i) \tag{7}$$

and solving for q , we obtain

$$q = LMR / \left((1/N) \sum_{i=1}^N p(x_i) \right). \tag{8}$$

We substituted q from Eq. (8) into Eq. (6) in order to infer local LMR at the resolution of the spatial prediction models from the regional average LMR value obtained from the calculated landslide volumes. We refer

to this process as “downscaling” of LMR because the result is a spatially differentiated prediction.

The above assumption of independence of landslide volume and probability of occurrence could only serve as a first-order approximation, and from a theoretical standpoint it was not obvious in which direction this assumption was more likely to be violated. On the one hand, mass movements might tend to be of greater magnitude at locations with a higher probability of occurrence because they are more unstable. On the other hand the contrary may be true because material may be released in more regular events for which less loose material is available. The assumption of independence of landslide magnitude and predicted probability of instability was therefore tested empirically.

4. Results

4.1. General characteristics of landslide types and distribution

Overall, the regional spatial landslide density in the Masamanaca area was greater than the cumulative density of the 1969–2000 period in the RBSF area (Fig. 3; Table 2); however, this has to be interpreted in the context of the persistence of landslide scars in each landscape, and the required landslide-generating period as discussed below. Masamanaca also had a much greater variety of landslide types than RBSF, as presented in more detail in the following sections.

4.1.1. Masamanaca area

The overall landslide density of all mass movement types in the Masamanaca area was higher in the Tertiary continental sediments than in metamorphic rocks (Table 2). However, median landslide areas were on average larger in the metamorphic part (see also Section 4.3; Table 2). In general a large variety of landslide types was observed. Twenty-one different mass movement types were identified (classified only with respect to type of movement according to Dikau et al., 1996). Complex slide-flows, flows and slides were the most abundant movement types in the study area (75% of all mass movements). Slumps, falls, topples and complex variations of these also exist, but with a far lower density (19% of all mass movements). We refer to a last landslide type as composite movements (6% of all mass movements). These are mostly large-scale movements

Table 2
Summary statistics of mass movements in the study area.

| | Masamanaca conglomerates | Masamanaca metamorphic | RBSF human ^a | RBSF natural ^a |
|--|--------------------------|------------------------|-------------------------|---------------------------|
| 3D Area (km ²) | 4.07 | 4.33 | 1.91 | 11.30 |
| All landslides | | | | |
| Total number of landslides | 536 | 220 | 138 | 691 |
| Number of landslide types | 6 | 6 | 3 | 3 |
| Regional landslide density (km ⁻²) | 132 | 51 | 14 ^b | 12 ^b |
| Mean (median) landslide size (m ²) | 1047 (512) | 1939 (997) | 1805 (938) | 793 (536) |
| Shallow and rainfall-triggered landslides | | | | |
| Number of landslides | 253 ^c | 77 ^c | 138 | 691 |
| Landslide density (km ⁻²) | 62 | 18 | 14 ^b | 12 ^b |
| Mean (median) landslide size (m ²) | 767 (491) | 1519 (936) | 1805 (938) | 793 (536) |

^a Values for five inventories (1969–2000). Only new landslide appearances (previous air photo acquisition was considered).

^b Average of landslide densities observed in each inventory.

^c Used for slope stability modeling and estimation of geomorphic process rates; in fact 575 landslides of the Masamanaca area (449 in the conglomerate part / 126 in the metamorphic rock part) were classified as shallow-slide, flow or slide-flow types but not all of them were rainfall-triggered.

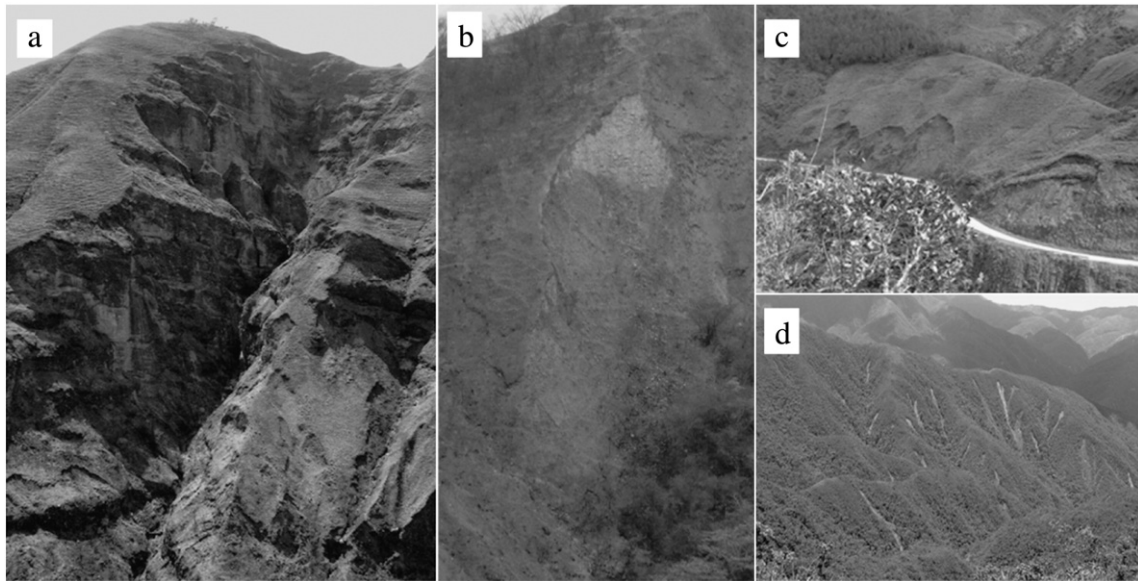


Fig. 4. Typical landslide types in the study areas. (a) Composite movement in Masanamaca. (b) Translational slide in Masanamaca. (c) Shallow landslides occurring along a road in the RBSF area. (d) Shallow landslides in the pristine mountain forest of the RBSF area.

formed by several movement types occurring either simultaneously or independently of each other (Fig. 4; Cruden and Varnes, 1996).

Rainfall events were considered to be the prevailing triggering factor in the Masanamaca area, especially of shallow movements (Fig. 5; Table 2). Fluvial and artificial debutting caused another 40% of the landslide population (Fig. 5). The initiation of large deep-seated movements such as composite landslides can likely be attributed to a combination of causative factors (Fig. 5). The importance of seismic activity as a trigger is difficult to assess without direct observations over time. However, the observed recent earthquake activity in southern Ecuador and lack of landslide occurrence after events of magnitudes 5.9 and 6.8 suggested that earthquakes were not a major triggering factor during the time period relevant to our study.

During the 5-year measurement period at the Vilcabamba weather station, in total at least one and up to six rainfall events exceeded the critical rainfall thresholds for shallow landslide initiation, depending on the empirical relationships used (see Section 3.2.1; Fig. 6; Table 3). Since major rain events may occur in different ENSO phases (Table 4) we assumed that rain events of similar intensity were likely to occur regularly, on average up to once per year. Since a single rainfall event would not produce the entire population of rainfall-induced shallow landslide scars that are visible, more than one potential rain event was necessary. With regard to the widespread existence of shallow movements and the fact that only a small number of young, scarcely revegetated slide scars could be identified in the field, we assumed that a period of several decades is required to generate a landslide population of the observed size.

Because of the substantial uncertainty we tentatively considered lower and upper bounds of the landslide-generating period of 10 and 100 years, respectively.

4.1.2. RBSF area

By contrast, landslides in the RBSF area were more uniformly shaped as elongated forms that were typical of the dominant shallow movements in this area, especially flows and slide-flows (Fig. 5). Wider and larger translational slides occurred only in direct contact with human-made structures such as the road and a power station in the northern part of the RBSF area (Figs. 2 and 5, Table 2); we refer to these as human-made landslides. These landslides are more frequently reactivated than the “natural” movements in the mountain forest which are subject to a fast regrowth and succession of vegetation (Richter, 2009). Within seven to nine years the majority of the natural landslides become unrecognizable in the field and in aerial photos (Stoyan, 2000).

Falls and topples were scarce along the San Francisco river (and were not explicitly mapped). Several rotational slides could be identified in the pastureland outside the study area. All mapped landslides in the RBSF study area were shallow landslides, which are generally triggered by rainfall events (Fig. 3; Aleotti, 2004; Giannecchini, 2006) or earthquakes (Tibaldi et al., 1995). Loading was limited to human activity and most often found along the road (Fig. 3). Debutting occurred along the road as well, but was more often detected in relation with fluvial erosion (Fig. 3). The large number of unidentified causative factors in the RBSF area was mainly due to difficult field access and the limitations

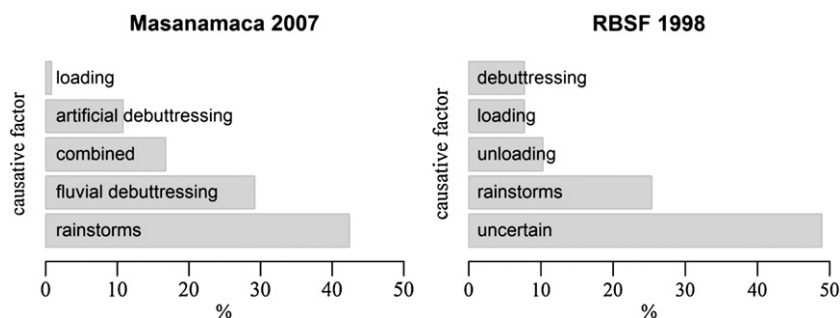


Fig. 5. Causative factors of mass movements according to field and aerial photo interpretation. Percentages include all mass movements including deep-seated ones.

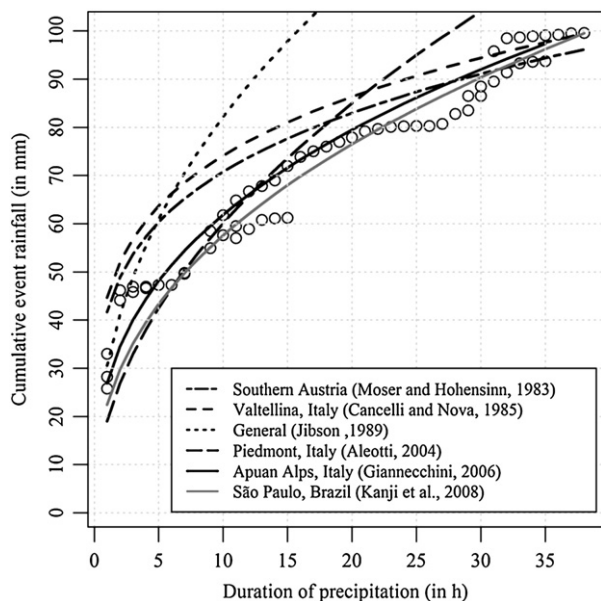


Fig. 6. Critical rainfall threshold curves compared with observed maximum precipitation events at the Vilcabamba weather station (circles; years 1998–2003). Note that a single rainfall event may be represented by several dots.

of aerial photo interpretation (Fig. 3). In other cases there was ambiguous field evidence.

4.2. Slope stability analysis

Among the four terrain attributes examined, the local slope angle and the size of the catchment area were the most closely related to landslide distribution in the four model areas, according to the univariate AUROC analysis and the deviance reduction achieved in the GAMs (Table 5). With the exception of the human-influenced part of the RBSF area, small contributing areas, i.e. essentially the upper part of the slopes, were more prone to landslide initiation (further discussed in Section 5.3.1), under otherwise equal topographic conditions controlled by the other predictor variables. Also, landslide initiation was more likely to occur on steep slopes, under otherwise equal conditions.

Convex slope profiles (positive profile curvatures) were more often associated with landslide initiation than concave ones (exception: natural part of the RBSF area). Convergent slopes (negative plan curvatures) in the Masamanaca conglomerates and the natural RBSF area in 2000 were much more prone to landsliding compared to parallel or divergent slopes according to the GAM; the influence of slope convergence was otherwise very weak. Distance to road,

Table 3
Number and duration of rainfall events exceeding empirically obtained critical precipitation thresholds for the 5-year observation period in Vilcabamba.

| Source of | Region | Number of rain events exceeding threshold | Rain duration (h) with threshold exceedence |
|----------------------------|-------------------|---|---|
| Moser and Hohensinn (1983) | Southern Austria | 1 | > 31 |
| Cancelli and Nova (1985) | Valtellina, Italy | 1 | > 31 |
| Jibson (1989) | Global | 2 | ≤ 2 |
| Aleotti (2004) | Piedmont, Italy | 4 | ≤ 12 |
| Giannecchini (2006) | Apuan Alps, Italy | 5 | 1–4 and 11–37 |
| Kanji et al. (2008) | São Paulo, Brazil | 6 | 1–38 |

Table 4
Maximum cumulative rain events at Vilcabamba (1998–2003) and corresponding ENSO episodes. During the observation period (1998–2003), 15 months corresponded to warm and 29 to cold ENSO episodes, and 18 months were non-ENSO periods. Warm and cold episodes based on a ± 0.5 °C threshold for the Oceanic Niño Index (ONI), based on the 1971–2000 base period. Source: National Weather Service Climate Prediction Center, http://www.cpc.ncep.noaa.gov/products/analysis_monitoring/ensostuff/ensoyears.shtml, accessed 21-Jun-2011.

| Date | Time | Duration (h) | Precipitation (mm) | ENSO episodes |
|----------------|-------|--------------|--------------------|---------------|
| 15-Apr-1998 | 21:00 | 4 | 46.6 | Warm episode |
| 16-Mar-1999 | 13:00 | 38 | 99.6 | Cold episode |
| 18-Mar-1999 | 16:00 | 1 | 25.8 | Cold episode |
| 26/27-Jan-2000 | 05:00 | 15 | 72 | Warm episode |
| 02/03-Apr-2001 | 01:00 | 7 | 49.6 | Cold episode |
| 26/27-Jan-2002 | 16:00 | 25 | 80.3 | None |
| 05/06-Mar-2002 | 10:00 | 35 | 93.7 | None |

the additional variable in the human-influenced RBSF area, was the strongest univariate and GAM predictor of landslide initiation in this subarea.

The GAM for the natural part of the RBSF area that used the newer, higher-quality DEM achieved a very good AUROC value of 88.0% on the training set and 84.2% in spatial cross-validation estimation (Table 6). The other GAMs produced a poorer goodness of fit (AUROC 65.4–75.2% on the training set, 55.3–71.9% in spatial cross-validation). Specifically in the Masamanaca conglomerates the GAM achieved a good AUROC value with slope and catchment area as the strongest predictors. The human-influenced RBSF area showed a similar good result, mainly due to the increased landslide activity along the road. We attribute the low AUROC value in the metamorphic part of the Masamanaca area to low DEM quality on slopes that had shadows during aerial photo acquisition, as the training-set AUROC value increased to 69.9% if the largest affected mountain slope was removed from the training set; the conglomerate area was less affected by such errors. In the RBSF area, the dependence of model performance on DEM quality suggests that the older DEM did not provide enough topographic detail compared to the photogrammetrically derived one. In the metamorphic part of the Masamanaca area and the human-influenced part of the RBSF area, bias-reduced cross-validation estimates of AUROC were up to 10% lower than in training-set estimation, which we attribute to the small sample sizes of training and test sets in these smaller areas with fewer landslides (Table 2). In the larger study areas, cross-validation estimates of AUROC were 1.6–3.8% lower than the corresponding training-set estimates, indicating very limited overfitting and a good transferability to adjacent test areas.

4.3. Geomorphic process rates

In the semi-arid Masamanaca area, the larger number of smaller mass movements in the conglomerate subarea resulted in nearly the same LMR values as in the metamorphic subarea (~0.4–4.4 vs. 0.3–2.6 mm yr⁻¹; ranges correspond to the upper and lower bound of landslide generating period; Table 7). However, the higher soil density and greater vertical material displacement in the metamorphic area led to significantly greater landslide-related geomorphic work and power compared to the conglomerates. Thus, in the latter area shallow landslide activity was more frequent, whereas the former is characterized by greater magnitudes and more significant material displacement.

LMR and geomorphic work in the metamorphic Masamanaca area and the natural part of RBSF were of a similar order of magnitude (0.3–2.6 vs. 2 mm yr⁻¹). LMR in the human-influenced part of the RBSF area, by contrast, was more than twice as high as in the natural RBSF area (2.0 vs. 4.7 mm yr⁻¹), which was a consequence of the larger mass movements that were attributed in many cases to human activities (Tables 2 and 7).

Table 5

Area under the ROC curve (AUROC) for each predictor variable, for the GAM, and for the SHALSTAB slope stability index, and relative deviance change associated with dropping one variable at a time from the GAM. Nonlinear predictors in the GAM are indicated with an asterisk (*). Deviance changes are expressed as percentages of null deviance.

| Variable / model | AUROC (%) | | | | | Deviance change (%) | | | | |
|-----------------------|---------------|----------------|---------------------|--------------|-----------------------|---------------------|----------------|---------------------|--------------|-----------------------|
| | Masam. congl. | Masam. metamo. | RBSF natural (2000) | RBSF natural | RBSF human-influenced | Masam. conglom. | Masam. metamo. | RBSF natural (2000) | RBSF natural | RBSF human-influenced |
| Slope | 64.2 | 53.3 | 77.4 | 58.1 | 50.6 | 4.1* | 0.2 | 13.8 | 1.1* | 2.1 |
| Log. catchment area | 68.8 | 62.9 | 53.2 | 57.7 | 56.3 | 3.8* | 2.9 | 3.4 | 1.7* | 2.1 |
| Plan curvature | 60.5 | 57.6 | 72.6 | 52.3 | 52.3 | 2.3 | 0.1 | 8.7* | 0.2 | 1.2* |
| Profile curvature | 64.9 | 61.1 | 64.0 | 53.7 | 55.1 | 1.7* | 1.1 | 0.2 | 0.2* | 1.1 |
| Log. distance to road | – | – | – | – | 60.0 | – | – | – | – | 9.8 |
| Elevation | – | – | 58.6 | 55.3 | – | – | – | 4.1* | 2.2* | – |
| GAM | 75.2 | 65.4 | 88.0 | 66.6 | 74.8 | 14.3 | 6.2 | 36.5 | 6.8 | 13.8 |
| SHALSTAB | 57.1 | 53.1 | 66.6 | 54.7 | 50.1 | – | – | – | – | – |

The spatial distribution of *LMR* within the study areas was down-scaled from the average rates using the empirical GAMs and Eqs. (6) and (8) (Fig. 7). As a measure of the degree of spatial differentiation in downscaled *LMR*, the average *LMR* value of the most landslide-prone 20% of the area in Masamanaca was 4.6 times higher than in the most stable 20% of the area. Note that this factor is independent of whether the upper or lower bound of the landslide generating period is adopted as it only depends on the contrast shown in the GAM predictions. In the natural RBSF area, the difference was 2.6-fold (2.7 vs. 1.1 mm yr⁻¹) when using the GAM for the older landslides and the smoother DEM, but it rose to a factor of 15 when using the GAM and DEM corresponding to the year 2000. This difference was not an artifact; it was related to the different discrimination achieved by the models (spatial cross-validation AUROC was 84.2% for the year 2000 and 65.0% for the earlier data; Table 6) and the different spatial scales represented by the DEMs in spite of an identical nominal raster resolution.

The assumption of independence of landslide magnitude and predicted probability of landslide initiation, which was made by the downscaling model, was supported by very weak correlations between predicted probabilities and estimated landslide thicknesses and volumes (absolute values of Spearman rank correlation coefficients and of Pearson correlations were <0.20 in all study areas).

5. Discussion

5.1. The study areas in a South American context

Our comparison of two contrasting study areas provided an insight into landslide distribution patterns and triggering mechanisms along a strong humidity gradient in a region that is strongly affected by a

Table 6

Model performance measured by AUROC and estimated on the training set and by non-spatial and spatial five-fold cross-validation. The interquartile range of AUROC over all 100 cross-validation replications is reported in parentheses.

| | AUROC – Median (IQR) (%) | | |
|-------------------------|--------------------------|------------------------------|--------------------------|
| | Training set | Non-spatial cross-validation | Spatial cross-validation |
| Masamanaca conglomerate | 75.2 | 73.4 (0.5) | 71.9 (0.6) |
| Masamanaca metamorphic | 65.4 | 59.4 (2.5) | 55.3 (2.6) |
| RBSF natural (2000) | 88.0 | 84.7 (0.5) | 84.2 (0.7) |
| RBSF natural | 66.6 | 65.8 (0.4) | 65.0 (0.6) |
| RBSF human-influenced | 74.8 | 73.0 (0.9) | 66.0 (1.6) |

variety of landslide types. At a regional scale, during the last millennium two of the five most devastating disasters associated with mass movements occurred in the Andean region (Evans, 2006). Some of the most catastrophic historic events are related to long-lasting heavy tropical rainfall events (e.g., debris flows in Venezuela, triggered by >900 mm precipitation within 3 days in December 1999; Genatios and Lafuente, 2003), high-magnitude earthquakes (e.g., Nevado Huascarán, Peru; Schuster et al., 2002, and Northern Ecuador; Tibaldi et al., 1995), or the activity of glaciated volcanoes (e.g., Nevado del Ruiz lahar, Colombia; Schuster et al., 2002), and thus reflect the enormous variety of climatic and geological triggering factors along the Andes. Postglacial adjustments of Pleistocene glacial topography to Holocene climate are an important preparatory factor in the other parts of the Andes, e.g., of Central Chile (Abele, 1981; Casassa and Marangunic, 1993).

So far such extreme geological or climatic hazards were not reported for our study areas. Neither do our areas present oversteepened glacial topographic conditions, nor recent volcanic activity (Litherland et al., 1994; Beck et al., 2008b) or high-magnitude earthquake activity (see Section 2). However, the regular occurrence of potentially landslide-triggering rainfall events, combined with steep slopes, strongly weathered rock types susceptible to failure (highly

Table 7

Volume, mass, mean vertical displacement and geomorphic process rates of shallow landslides in both study areas. Uncertainties in volume estimation are discussed in Section 3.2.1; they propagate into estimates of geomorphic activity.

| | Masamanaca conglomerates | Masamanaca metamorphic | RBSF natural ^a | RBSF human ^a |
|---|--------------------------|------------------------|---------------------------|-------------------------|
| Volume (m ³ km ⁻²) | 44208 | 25746 | 58809 | 160793 |
| Mass (kt km ⁻²) | 57 | 36 | 82 | 225 |
| Volume per year (m ³ km ⁻² yr ⁻¹) | 4421 | 2575 | 2003 | 4661 |
| Mass per year (kt km ⁻² yr ⁻¹) | 0.6–6 | 0.4–4 | 3 | 7 |
| Mean vertical displacement (m) | 7 | 18 | 27 | 26 |
| Geomorphic activity | | | | |
| Total work (MJ km ⁻²) | 7673 | 12459 | 35254 | 84439 |
| Power (MJ yr ⁻¹ km ⁻²) | 77–767 | 125–1246 | 1236 | 2229 |
| Power (W km ⁻²) | 2–24 | 4–39 | 39 | 71 |
| Mobilization rate (mm yr ⁻¹) | 0.4–4.4 | 0.3–2.6 | 2.0 | 4.7 |

^a Average values of five inventories (1969–2000). Only new landslide appearances (previous air photo acquisition was considered). In order to obtain results relative to the planimetric surface area rather than the “true” 3D area, multiply the values in this table with 1.20 (RBSF natural, RBSF human), 1.07 (Masamanaca conglomerates) and 1.13 (Masamanaca metamorphic), respectively.

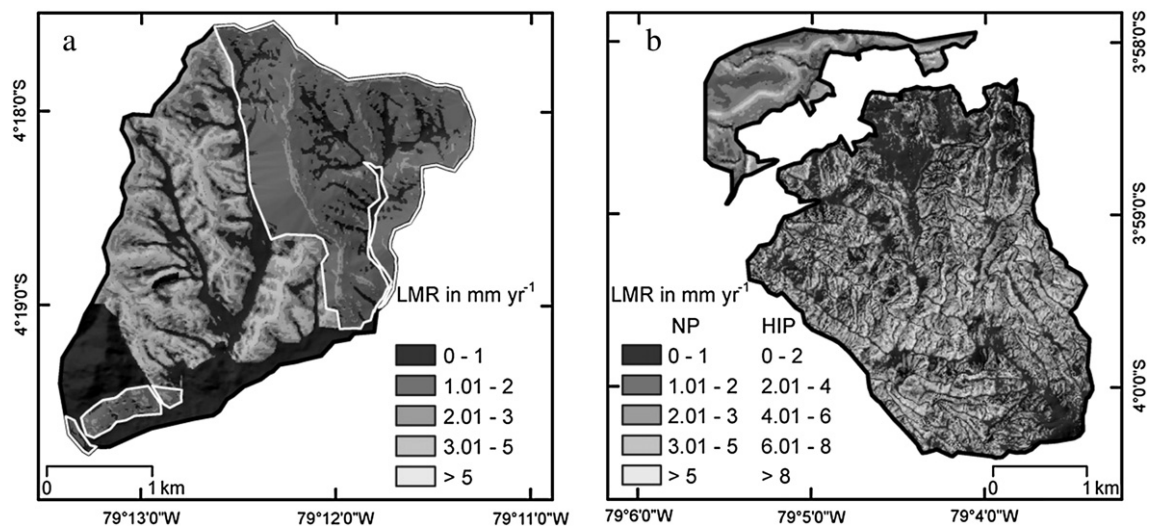


Fig. 7. Landslide mobilization rate (*LMR*) of shallow landslides in (a) Masamanaca (area underlain by metamorphic rock is delineated by a white line) and (b) the RBSF area (NP: northern natural part; HIP: southern human influenced part, separated by an offset b). The estimated mean values of *LMR* for each area corresponds to Table 7; for Masamanaca, 4.4 and 2.6 mm yr⁻¹ were used for conglomerate and metamorphic parts, respectively.

schistous phyllites and conglomerates) and seismic activity, provide the conditions for developing large numbers of mass movements with considerable material mobilization (Stoyan, 2000; Wilcke et al., 2003; Emck, 2007; Beck et al., 2008b). Consequently, both our study regions are geomorphologically very active zones compared to different mountain environments worldwide (Tables 7 and 8).

5.2. Quantitative comparisons in both study areas and on a global scale

5.2.1. Comparison of *LMRs*

The spatial patterns of landslide initiation were used to infer the spatial differentiation of *LMR* within the study areas (Fig. 7), which constitutes a novel approach for downscaling process rates that may be applicable in the broader context of mesoscale sediment budget modeling.

Within a century the Masanamca conglomerates may experience a vertical surface lowering of the order of 30–50 cm caused by shallow

landsliding. By contrast, the less landslide-prone metamorphic part will likely only face about 20 cm lowering during the same time period (Fig. 7). This difference is even more pronounced between the human-influenced and the natural part of the RBSF. Along the road a lowering of almost 1 m may take place during a 100-year period if the mobilized material is also removed. By contrast, areas in the natural part of the RBSF area at the same altitudinal level will likely be much less affected by surface lowering (~0–20 cm; Fig. 7).

Overall, the spatial pattern of surface lowering rates will tend to further incise and steepen already steep convergent hillslopes, creating a positive feedback mechanism that may, over centuries (Masamanaca: badland development) or millennia (natural part of RBSF area), lead to the development of V-shaped valleys, and thus contribute to landscape evolution (Fig. 8).

While the *LMR* values of shallow mass movements in the Masamanaca and natural RBSF area were similar in magnitude, the total mobilization rate of all mass movement types in the Masamanaca area is presumably

Table 8
Comparison of landslide mobilization rates (*LMR*) for different regions worldwide.

| Author | Location | Average <i>LMR</i> in mm/yr | Landslide type | Landuse | Geology | Main triggers |
|--------------------------------|--|-----------------------------|--|---|--|--|
| Korup et al. (2005) | Western Southern Alps (New Zealand) | 9.1 ± 5.1 | Shallow landslides | n. a. | Schists | Climatic and seismic |
| Hovius et al. (1997) | Western Southern Alps (New Zealand) | 9 ± 4 | Fall, slump, (rock) slide, debris flow | n. a. | Schists and gneisses | Climatic and seismic |
| Guzzetti et al. (2009) | Umbria (Central Italy) | 8.8 | Slide type | n. a. | Sedimentary rocks | Chiefly intense and prolonged rainfall, snowmelt |
| Barnard et al. (2001) | Garhwal, Himalaya (northern India) | 0.6–6 | Mainly shallow landslides | Human activity accelerates denudation | Medium-grade metamorphic rocks | Earthquake and rainfall |
| This study | RBSF – human-influenced part (Ecuador) | ~5 | Shallow landslides | Pastureland and road | Metamorphic rock | Rainfall |
| This study | Masanamaca (Ecuador) | 0.4–4 | Shallow landslides | Pastureland, regular burning | Conglomerates and metamorphic rock | Rainfall |
| This study | RBSF – natural part (Ecuador) | 2 | Shallow landslides | None | Metamorphic rock | Rainfall |
| Molina et al. (2008) | Paute basin (Ecuador) | 0.6–1.4 ^a | Sediment yield of two catchments | Domination of urban and agricultural land | Mostly sand-, siltstone, conglomerates | n. a. |
| Gerrard and Gardner (2002) | Likhu Khola drainage basin, Middle Hills (Nepal) | 0.44 | Slumps and debris slides | Mostly agricultural (terraced) land | Largely gneisses | Rainfall |
| Lewkowicz and Hartshorn (1998) | Sawtooth Range, Ellesmere Island (Canada) | 0.07 | Debris flows | None | Lime-, silt- and sandstone | Climatic |

^a Rate based on sediment volumes measured behind check dams (data for two catchments, corresponding pretty well to the physiographical setting of the conglomerate part of Masanamaca, additionally provided by courtesy of Molina, A., 2009).

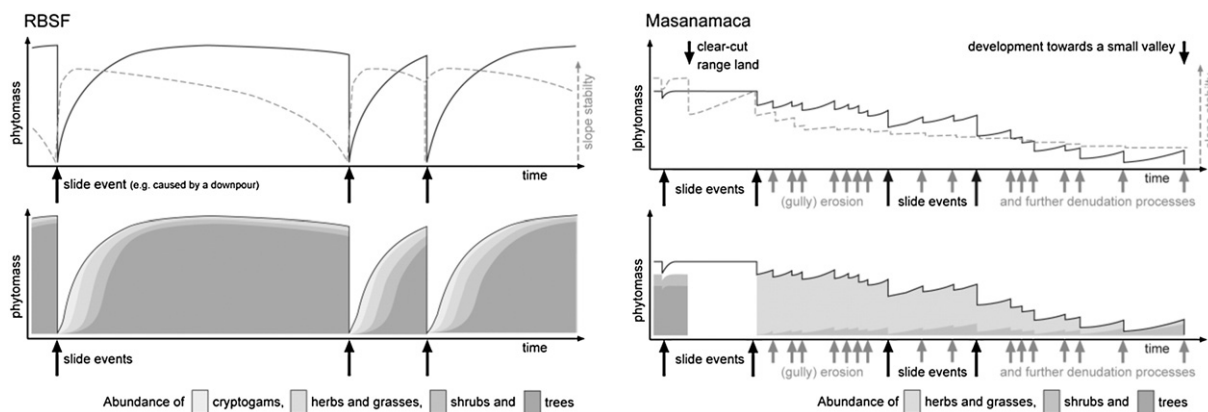


Fig. 8. Conceptual model of vegetation succession on landslides in both study areas and their implications for landscape evolution (modified after Richter, 2009). In the wet mountain rainforest (RBSF), landslides are part of a cycle initiating the return to the original state, whereas in Masanamaca, landslides tend to initiate a stepwise ecosystem degradation due to the loss of phytomass.

substantially higher given the large number of deep-seated landslides, for which we did not estimate volumes and recurrence intervals. Slopes affected by these movements are now in an advanced stage of progressive slope retreat leading to surface lowering, which could have had its origin in a small landslide scar. This assumption found support through the comparison of aerial photos (1962 and 2000) with the field-mapped landslide inventory of 2007/08.

The average catchment-scale fluvial sediment yield in a similar area ca. 200 km north of Masanamaca is 2.9 mm yr^{-1} (average of 17 catchments in the Cuenca intermontane basin; Table 1 in Molina et al., 2008). Sediment yield in catchments with low vegetation cover (especially when $<25\%$) was significantly increased (average denudation rate 7.8 mm yr^{-1} compared to 1.4 mm yr^{-1} in areas with denser vegetation; Molina et al., 2008).

5.2.2. Comparison of geomorphic work and power

Only a few comparable studies have dealt with geomorphic work and power, which limits the possibilities for contrasting these process rates between different mountain areas. Geomorphic power would otherwise be a more suitable measure for quantitatively comparing the geomorphic significance of different landslide types and other erosion processes (Caine, 1976). The geomorphic power of $11.4 \text{ MJ yr}^{-1} \text{ km}^{-2}$ for mudflows calculated after Caine (1976) for a small exemplary area in the San Juan Mountains (Colorado, USA) is at least one order of magnitude lower than for shallow landslides in the Masanamaca area, and at least two orders of magnitude lower than in the RBSF area (Table 7). Debris flows in Arctic Canada, by contrast, account for significantly lower geomorphic power ($0.4 \text{ MJ yr}^{-1} \text{ km}^{-2}$; after Lewkowitz and Hartshorn, 1998). On the other hand, the work calculated by Shroder (1998) for individual and multiple slope failures in the western Himalaya possibly exceeds the values obtained in our study, but is difficult to compare numerically because all calculations were conducted without reference to a time unit. These comparisons show that it would be desirable to make broader use of the concepts of geomorphic work and power to express surface lowering processes quantitatively. Comparable process rates from South America are not available, and further research is therefore needed to make more focused comparison regionally and worldwide.

Temporal landslide frequencies may exhibit strong fluctuations over time as a function of the (largely random) number of landslide-triggering events such as high-intensity rainfall events or earthquakes occurring during a given observation period, with obvious consequences for uncertainties in the estimation of process rates in time. Naturally, landslide inventories only provide a snapshot, both spatially and temporally, of landslide activity and process rates. Both longer-term, regional-scale monitoring and detailed in situ investigations are needed to obtain more accurate estimates of these rates.

5.3. Local patterns and controls, and landscape evolution under human pressure

5.3.1. Influence of predictor variables on shallow landsliding according to GAM

The modeling revealed certain characteristics typical for shallow landslide initiation (see Section 4.2). For instance, small contributing areas coincided with convex slope profiles as less stable topographic positions in the Masanamaca area and with concave slope profiles in the natural part of the RBSF area. We provide a tentative geomorphic interpretation of these patterns. In the first case, smaller contributing areas, which are mainly located on the upper slopes near the divides, may be affected by increased infiltration on a slope shoulder, as expressed by the convex profile curvature. Consequently, an increasing pore water pressure reduces shear strength to the point of failure especially on steep slopes, e.g., directly beneath the slope shoulder in convex slope profiles. By contrast, in the natural part of the RBSF area, locations with concave slope profiles mostly had small upslope contributing areas and slope angles greater than the friction angle, according to exploratory data analyses (not shown); a large portion of these locations were affected by shallow landsliding. Thus, in accordance with the model results, the steep upper concave slope profiles in proximity to the ridges were most landslide-prone in the natural RBSF area.

5.3.2. Human pressure

Human activities appeared to exert a strong influence on landsliding in both study areas. Despite lower rainfall intensities and in the light of estimation uncertainties, it seemed that the LMR of the deforested metamorphic part of the Masanamaca area reached a similar LMR as the natural RBSF part (Table 7). Regular burning was also present, which may lower the critical threshold needed for the triggering of shallow landslides (Cannon and Gartner, 2005), and probably affected the conglomerate part even more than the metamorphic part of the Masanamaca area, visible in a higher regional landslide density (Table 2). Human activities are also known to have accelerated erosion rates drastically (Hewawasam et al., 2003; Vanacker et al., 2007b). Likewise Molina et al. (2008) reported the gradual transition into badlands in parts of a comparable study area located further north in Ecuador, if not revegetated.

Similarly, the overwhelming influence of road construction (built in 1962) and associated land use and deforestation in the human-influenced part of the RBSF area was evident in the field and clearly reflected by our quantitative results. Since a revegetation and restabilization of these oversteepened road cuts and head scarps appeared unlikely under the given topographic and land use conditions, we suggest that a sequence of mass movements may possibly lead to the long-term development of badlands similar to the ones found in

the metamorphic Masamanaca area. However, we anticipate that this landscape degradation may likely evolve more quickly in the human-influenced RBSF area due to higher precipitation values leading to more dissected, oversteepened and therefore partly regolith-free slopes with shallow movements successively changing into larger and deeper ones.

5.4. Relationships between landslides and vegetation

5.4.1. Influence of vegetation on slope stability

Vegetation may exert an important influence on slope stability in general as well as in our study areas, especially the RBSF area (Restrepo et al., 2009; Gao and Maro, 2010). Hydrological and mechanical effects of vegetation can be distinguished (Roering et al., 2003; Marston, 2010). Tree canopies may smooth precipitation intensities, which may result in an increased stability under forest canopies with greater interception capacity (Keim and Skaugset, 2003). Ground cover may play a similar role (Gabet and Dunne, 2002; Stokes et al., 2007; Vanacker et al., 2007a; Molina et al., 2008). In the RBSF area, canopy structure and ground cover type both vary greatly between the altitudinal vegetation zones. For example, between 2100 and 2750 m a.s.l., the one-storey tree stratum upper mountain forest replaces the two-storey tree stratum lower mountain rainforest. In the transition from upper mountain forest to páramo at 2700–3000 m a.s.l. the canopy becomes extremely dense again, even though it is formed by treelet species with only 1–2 m wide, small crowns. Also, the occurrence of thick carpets of mosses may reduce infiltration into the soil in this belt (Bussmann, 2004; Homeier et al., 2008). We speculate that such altitudinal changes in vegetation characteristics that influence hillslope hydrology may at least partly be reflected by the observed influence of elevation in the GAMs of the natural RBSF area, where elevations around 2400 m a.s.l. were highlighted as most unstable. However, the altitudinal increase in mean precipitation (Emck, 2007) and local variation of slope angles may act as confounders, and therefore detailed field-scale studies may be necessary to separate these possible influences.

On a local scale, destabilized trees and fire may open up gaps that become exposed to rainfall without a protective tree canopy (Bussmann, 2004) and lateral root reinforcement (Schwarz et al., 2010). Regarding the mechanical effects of vegetation, the mechanical transmission of dynamic forces of wind to the soil (Sidle and Ochiai, 2006) would more likely have an effect near the ridges (Soethe et al., 2006). This is consistent with our empirical findings that landslide initiation in the RBSF area is more likely in the upper reaches of hillslopes near the ridges, and altitudinally in the middle parts of the upper mountain rainforest (Bussmann, 2004). Another potential mechanical influence of vegetation that has been put forward in this area is the large accumulation of plant biomass during vegetation succession towards a mature mountain rainforest (Restrepo et al., 2009; Gao and Maro, 2010). Although the individual contributions of these hydrological and mechanical effects of vegetation on the stability of hillslopes could not be determined in this study, they are likely of importance in the tropical mountain forest environments (Restrepo et al., 2009), and they are at least implicitly captured by the empirical relationships in our slope stability models.

5.4.2. Plant succession on landslides

Landslide-related vegetation disturbance patterns vary spatially as described above, and plant succession and ultimately land degradation in each study area is also influenced by land use and the substantial differences in rainfall frequency and intensity (see Section 2; Fig. 2; Emck, 2007). In the natural RBSF area a relatively fast “mosaic cycle” of the mountain rainforest ecosystem initializes on the bare landslide-affected ground (Fig. 8; Richter, 2009). First pioneers are cryptogams including algae and fungi, establishing a seedbed for following grasses, herbs and ferns (Bussmann et al., 2008). Only a few

years later a dense vascular plant coverage protects the ground from further soil erosion, thus enhancing slope stability (Hagedorn, 2001). Finally an upcoming secondary forest gradually turns into a mature stand, presumably heavy enough to cause slope failure in conjunction with high soil water contents and changing flow patterns along shear zones (Fig. 8).

By contrast, in the semi-arid Masanamaca area only a very slow succession can be observed. Often plant development remains in pre-mature stages. Human-made fires preceding the rainy season, not only interrupt but strongly hamper the reestablishment of vegetation. Additionally, the dry season suppresses the appearance of mosses and lichens, both essential initial founders of vascular plant growth and its consolidating root system. Consequently, especially scarps of steep translational slides remain exposed to rainfall, which benefits gully erosion and badland development (Richter, 2009).

While landslides in the Masanamaca area lead successively to land degradation accompanied by a loss of species richness, in the natural part of the perhumid RBSF they contribute to the outstanding plant diversity, granting a refuge to plant species and genera, mainly of the herbaceous and shrub layer, which in a mature mountain rainforest cannot withstand the competition (Wilcke et al., 2003; Lozano et al., 2005; Beck et al., 2008a; Bussmann et al., 2008; Richter, 2009).

6. Conclusions

Our comparative study in semi-arid and humid areas of the tropical Andes of Southern Ecuador revealed a considerable diversity of landslide types as well as high geomorphic process rates associated with landslide activity. Human disturbances including road construction, deforestation and burning of vegetation enhanced landslide activity in these areas. Thus, the human-influenced part of the humid RBSF area reached highest process rates ($LMR \approx 5 \text{ mm yr}^{-1}$), which was mainly due to landslides occurring along a road, and was more than twice as high as in the natural part of the RBSF area ($LMR = 2 \text{ mm yr}^{-1}$). In the natural RBSF area, natural vegetation successions were both the result and presumably a causing factor of landslides; the latter due to vegetation overload and wind effects. These successions also contribute to species richness in this hot spot of phytodiversity. Process rates estimated for the semi-arid Masanamaca area are still subject to substantial uncertainties due to limited information on landslide age and the frequency of critical rainfall intensities. LMR in these deforested areas appeared to be of a similar magnitude as in the natural RBSF area.

Downscaled LMR values obtained from GAMs as semi-parametric empirical–statistical landslide susceptibility models provided novel insights into the spatial distribution of landslide activity and denudation. This additional spatial differentiation was useful for identifying areas of increased landscape evolution and degradation under the current land use conditions.

Acknowledgment

We are grateful to Dr. Frank Haubrich for providing soil data and valuable discussion on soil properties in the RBSF area, and to Dr. E. Jordan and M.A. Lars Ungerechts for providing remote sensing data. We would like to thank Armando Molina for providing additional data for comparison with his work. We also would like to express our gratitude to Dr. Fausto Guzzetti and another anonymous reviewer for constructive comments that helped to improve the paper. Financial support from the Deutsche Forschungsgemeinschaft (Research Unit 816) and Natural Sciences and Engineering Research Council of Canada (Discovery Grant – Individual) is gratefully acknowledged.

References

- Abele, G., 1981. Trockene Massenbewegungen, Schlammströme und rasche Abflüsse. Dominante morphologische Vorgänge in den chilenischen Anden. *Mainzer Geographische Studien* 23, Mainz.
- Aleotti, P., 2004. A warning system for rainfall-induced shallow failures. *Engineering Geology* 73, 247–265.
- Atkinson, P.M., Massari, R., 2011. Autologistic modelling of susceptibility to landsliding in the Central Apennines, Italy. *Geomorphology* 130, 55–64.
- Barnard, P.L., Owen, L.A., Sharma, M.C., Finkel, R.C., 2001. Natural and human-induced landsliding in the Garhwal Himalaya of northern India. *Geomorphology* 40, 21–35.
- Barthlott, W., Hostert, A., Kier, G., Küper, W., Kreft, H., Mutke, J., Rafiqpoor, D., Sommer, J.H., 2007. Geographic patterns of vascular plant diversity at continental to global scales. *Erdkunde* 61, 305–315.
- Beck, E., Bendix, J., Kottke, I., Makeschin, F., Mosandl, R. (Eds.), 2008a. Gradients in a Tropical Mountain Ecosystem of Ecuador. Springer, Berlin, Heidelberg.
- Beck, E., Makeschin, F., Haubrich, F., Richter, M., Bendix, J., Valerezo, C., 2008b. The ecosystem (Reserva Biológica San Francisco). In: Beck, E., Bendix, J., Kottke, I., Makeschin, F., Mosandl, R. (Eds.), *Gradients in a Tropical Mountain Ecosystem of Ecuador*. Springer, Berlin, Heidelberg, pp. 1–14.
- Brenning, A., 2005. Spatial prediction models for landslide hazards: review, comparison and evaluation. *Natural Hazards and Earth System Sciences* 5, 853–862.
- Brenning, A., 2008. Statistical geocomputing combining R and SAGA: The example of landslide susceptibility analysis with generalized additive models. In: Böhner, J., Blaschke, T., Montanarella, L. (Eds.), *SAGA – Seconds Out (= Hamburger Beiträge zur Physischen Geographie und Landschaftsökologie, 19)*, Hamburg, pp. 23–32.
- Brenning, A., 2009. Benchmarking classifiers to optimally integrate terrain analysis and multispectral remote sensing in automatic rock glacier detection. *Remote Sensing of Environment* 113, 239–247.
- Bussmann, R., 2004. Regeneration and succession patterns in African, Andean and Pacific tropical mountain forests: the role of natural and anthropogenic disturbance. *Lyonia* 6, 93–111.
- Bussmann, R.W., Wilcke, W., Richter, M., 2008. Landslides as important disturbance regimes – causes and regeneration. In: Beck, E., Bendix, J., Kottke, I., Makeschin, F., Mosandl, R. (Eds.), *Gradients in a Tropical Mountain Ecosystem of Ecuador*. Springer, Berlin, Heidelberg, pp. 319–330.
- Caine, N., 1976. A uniform measure of subaerial erosion. *Geological Society of America Bulletin* 87, 137–140.
- Caine, N., 1980. The rainfall intensity: duration control of shallow landslides and debris flows. *Geografiska Annaler. Series A Physical Geography* 62, 23–27.
- Cancelli, A., Nova, R., 1985. Landslides in soil debris cover triggered by rainfall in Valtellina (Central Alps, Italy). *Proceedings of the 4th International Conference on Landslides*, Tokyo, vol. 1. A. A. Balkema Publishers, Rotterdam, pp. 267–272.
- Cannon, S.H., Gartner, J.E., 2005. Wildfire-related debris flow from a hazards perspective. In: Jakob, M., Hungr, O. (Eds.), *Debris-flow Hazards and Related Phenomena*. Springer, Berlin, Heidelberg, pp. 363–385.
- Casassa, G., Marangunic, C., 1993. The 1987 Rio Colorado rockslide and debris flow, Central Andes, Chile. *Bulletin of the Association of Engineering Geologists* 30, 321–330.
- Crosta, G.B., Frattini, P., 2001. Rainfall thresholds for triggering soil slips and debris flow. *Proceedings of the 2nd Plinius International Conference on Mediterranean Storms*, Siena, Italy, pp. 463–487.
- Crozier, M.J., 1984. Field assessment of slope instability. In: Brunson, D., Prior, D.B. (Eds.), *Slope Instability*. Wiley, Chichester, pp. 103–142.
- Crozier, M.J., 1986. Landslides: Causes, Consequences & Environment. Croom Helm, London.
- Cruden, D.M., Varnes, D.J., 1996. Landslide types and processes. In: Turner, A.K., Schuster, R.L. (Eds.), *Landslides: Investigation and Mitigation*. National Academic Press, Washington, DC, pp. 36–75.
- Dikau, R., Brunson, D., Schrott, L., Ibsen, M.L. (Eds.), 1996. *Landslide Recognition: Identification, Movement and Causes*. Wiley, Chichester.
- Efron, B., Gong, G., 1983. A leisurely look at the bootstrap, the jackknife, and cross-validation. *The American Statistician* 37, 36–48.
- Emck, P., 2007. A climatology of South Ecuador. With special focus on the major Andean Ridge as Atlantic-Pacific climate divide. Ph.D. thesis, University of Erlangen-Nuremberg, Germany.
- Evans, S.G., 2006. Single-event landslides resulting from massive rock slope failure: characterizing their frequency and impact on society. In: Evans, S.G., Mugnoz, G.S., Strom, A., Hermanns, R.L. (Eds.), *Landslides from Massive Rock Slope Failure*. Proceedings of the NATO Advanced Research Workshop on Massive Rock Slope Failure – New Models for Hazard Assessment, Celano, Italy, 16–21 June 2002. Springer, Berlin, pp. 53–73.
- Gabet, E.J., Dunne, T., 2002. Landslides on coastal sage-scrub and grassland hillslopes in a severe El Niño winter: the effects of vegetation conversion on sediment delivery. *Geological Society of America Bulletin* 114, 983–990.
- Gao, J., Maro, J., 2010. Topographic controls on evolution of shallow landslides in pastoral Wairarapa, New Zealand, 1979–2003. *Geomorphology* 114, 373–381.
- Genatios, C., Lafuente, M., 2003. Lluvias torrenciales en Vargas, Venezuela, en diciembre de 1999. *Protección medioambiental y recuperación urbana. Boletín técnico IMME* 41, 49–62.
- Gerrard, J., Gardner, R., 2002. Relationships between landsliding and land use in the Likhu Khola Drainage Basin, Middle Hills, Nepal. *Mountain Research and Development* 22, 48–55.
- Giannacchini, R., 2006. Relationship between rainfall and shallow landslides in the southern Apuan Alps (Italy). *Natural Hazards and Earth System Sciences* 6, 357–364.
- Goetz, J.N., Guthrie, R.H., Brenning, A., 2011. Integrating physical and empirical landslide susceptibility models using generalized additive models. *Geomorphology* 129, 376–386.
- Guffroy, J., 2006. El horizonte corrugado: correlaciones estilísticas y culturales. *Bulletin de l'Institut Français d'Études Andines* 35, 347–359.
- Guzzetti, F., Peruccacci, S., Rossi, M., Stark, C.P., 2008. The rainfall intensity-duration control of shallow landslides and debris flows: an update. *Landslides* 5, 3–17.
- Guzzetti, F., Ardizzone, F., Cardinali, M., Rossi, M., Valigi, D., 2009. Landslide volumes and landslide mobilization rates in Umbria, central Italy. *Earth and Planetary Science Letters* 279, 222–229.
- Hagedorn, A., 2001. Extent and significance of soil erosion in southern Ecuador. *Erde* 132, 75–92.
- Hagedorn, A., 2002. Erosionsprozesse in Südecuador unter besonderer Berücksichtigung des Oberflächenabtrags. Unpublished Ph.D. thesis, University of Erlangen-Nuremberg, Germany.
- Hastie, T., 2009. Gam: Generalized Additive Models. R Package Version 1.0.1.
- Haubrich, F., Makeschin, F., Unger, M., Abiy, M., Burneo, J. I., submitted. Land use effects on carbon and nitrogen stocks and natural isotope C and N signatures in a tropical mountain ecosystem in South Ecuador. Submitted to *Soils and Sediments*.
- Hewawasam, T., von Blanckenburg, F., Schaller, M., Kubik, P., 2003. Increase of human over natural erosion rates in tropical highlands constrained by cosmogenic nuclides. *Geology* 31, 597–600.
- Homeier, J., Werner, F.A., Gradstein, S.R., Breckle, S.-W., Richter, M., 2008. Potential vegetation and floristic composition of Andean forests in South Ecuador, with a focus on the RBSF. In: Beck, E., Bendix, J., Kottke, I., Makeschin, F., Mosandl, R. (Eds.), *Gradients in a Tropical Mountain Ecosystem of Ecuador*. Springer, Berlin, Heidelberg, pp. 87–100.
- Hovius, N., Stark, C.P., Allen, P.A., 1997. Sediment flux from a mountain belt derived by landslide mapping. *Geology* 25, 231–234.
- IGEPN, 2011. Servicio Nacional de Sismología y Vulcanología. <http://www.igepn.edu.ec> (last accessed on 21 June 2011).
- Jibson, R.W., 1989. Debris flows in Southern Puerto Rico. In: Schultz, A.P., Jibson, R.W. (Eds.), *Landslide Processes of the Eastern United States and Puerto Rico: Geological Society of America Special Paper*, 236, pp. 29–55 (Boulder, CO).
- Kanji, M.A., Cruz, P.T., Massad, F., 2008. Debris flow affecting the Cubatao Oil Refinery, Brazil. *Landslides* 5, 71–82.
- Keim, R.F., Skaugset, A.E., 2003. Modelling effects of forest canopies on slope stability. *Hydrological Processes* 17, 1457–1467.
- Korup, O., Schmidt, J., McSaveney, M.J., 2005. Regional relief characteristics and denudation pattern of the western Southern Alps, New Zealand. *Geomorphology* 71, 402–423.
- Larsen, I.J., Montgomery, D.R., Korup, O., 2010. Landslide erosion controlled by hillslope material. *Nature Geoscience* 3, 247–251.
- Lewkowicz, A.G., Hartshorn, J., 1998. Terrestrial record of rapid mass movements in the Sawtooth Range, Ellesmere Island, Northwest Territories, Canada. *Canadian Journal of Earth Sciences* 35, 55–64.
- Litherland, M., Aspden, J.A., Jemielita, R.A., 1994. *The Metamorphic Belts of Ecuador*. British Geological Survey, Bath, UK.
- Lozano, P., Bussmann, R.W., Küppers, M., 2005. Landslides as ecosystem disturbance – their implications and importance in South Ecuador. *Lyonia* 8, 67–72.
- Marston, R.A., 2010. Geomorphology and vegetation on hillslopes: interactions, dependencies, and feedback loops. *Geomorphology* 116, 206–217.
- Molina, A., Govers, G., Poesen, J., van Hemelryck, H., de Bievre, B., Vanacker, V., 2008. Environmental factors controlling spatial variation in sediment yield in a central Andean mountain area. *Geomorphology* 98, 176–186.
- Moser, M., Hohensinn, F., 1983. Geotechnical aspects of soil slips in Alpine regions. *Engineering Geology* 19, 185–211.
- Park, N.W., Chi, K.H., 2008. Quantitative assessment of landslide susceptibility using high-resolution remote sensing data and a generalized additive model. *International Journal of Remote Sensing* 29, 247–264.
- Peters, T., Diertl, K.-H., Gawlik, J., Rankl, M., Richter, M., 2010. Vascular plant diversity in natural and anthropogenic ecosystems in the Andes of Southern Ecuador: studies from the Rio San Francisco valley. *Mountain Research and Development* 30, 344–352.
- Prinz, H., Strauß, R., 2006. *Abriss der Ingenieurgeologie*. Elsevier, Spektrum Akad. Verl., München.
- Restrepo, C., Walker, L.R., Shiels, A.B., Bussmann, R., Claessens, L., Fisch, S., Lozano, P., Negi, G., Paolini, L., Poveda, G., Ramos-Scharron, C., Richter, M., Velazquez, E., 2009. Landsliding and its multiscale influence on mountainscapes. *Bioscience* 59, 685–698.
- Richter, M., 2009. To what extent do natural disturbances contribute to Andean plant diversity? A theoretical outline from the wettest and driest parts of the tropical Andes. *Advances in Geosciences* 22, 95–105.
- Riemer, W., Ruppert, F.R., Locher, T.C., Nuñez, I., 1989. Regional assessment of slide hazards. *Proceedings of the 5th International Symposium on Landslides*, 10–15 July 1988, Lausanne, pp. 1223–1226.
- Roering, J.J., Schmidt, K.M., Stock, J.D., Dietrich, W.E., Montgomery, 2003. Shallow landsliding, root reinforcement, and the spatial distribution of trees in the Oregon Coast Range. *Canadian Geotechnical Journal* 40, 237–253.
- Rossel, F., Cadier, E., 2009. El Niño and prediction of anomalous monthly rainfalls in Ecuador. *Hydrological Processes* 23, 3253–3260.
- Ruß, G., Brenning, A., 2010. Data mining in precision agriculture: management of spatial information. *Lecture Notes in Computer Science* 6178, 350–359.
- Schubert, C., 1999. *Klassifikation, Genese und Standorteigenschaften tropischer Gebirgsböden im Lee der Cordillera Real, Südecuador*. Unpublished Diploma Thesis, University of Bayreuth, Germany.
- Schuster, R.L., Salcedo, D.A., Valenzuela, L., 2002. Overview of catastrophic landslides of South America in the twentieth century. In: Evans, S.G., DeGraff, J.V. (Eds.),

- Catastrophic Landslides: Effects, Occurrence, and Mechanisms. The Geological Society of America, Boulder, CO, pp. 1–34.
- Schwarz, M., Lehmann, P., Or, D., 2010. Quantifying lateral root reinforcement in steep slopes – from a bundle of roots to tree stands. *Earth Surface Processes and Landforms* 35, 354–367.
- Shroder Jr., J.F., 1998. Slope failure and denudation in the western Himalaya. *Geomorphology* 26, 81–105.
- Sidle, R.C., Ochiai, H., 2006. Landslides. Processes, Prediction, and Land Use. American Geophysical Union, Washington, DC.
- Soethe, N., Lehmann, J., Engels, C., 2006. Root morphology and anchorage of six native tree species from a tropical montane forest and an elfin forest in Ecuador. *Plant and Soil* 279, 173–185.
- Stokes, A., Spanos, I., Norris, J.E., Cammeraat, E. (Eds.), 2007. Eco- and Ground Bio-engineering. The Use of Vegetation to Improve Slope Stability. Proceedings of the First International Conference on Eco-Engineering 13–17 September 2004. Springer, Dordrecht.
- Stoyan, R., 2000. Aktivität, Ursachen und Klassifikation der Rutschungen in San Francisco/Südecuador. Unpublished Diploma Thesis, University of Erlangen-Nuremberg, Germany.
- Tibaldi, A., Ferrari, L., Pasquare, G., 1995. Landslides triggered by earthquakes and their relations with faults and mountain slope geometry – an example from Ecuador. *Geomorphology* 11, 215–226.
- USGS, 2011. Earthquake Hazards Program. <http://earthquake.usgs.gov/> (last accessed on 21 June 2011).
- Vanacker, V., von Blanckenburg, F., Govers, G., Molina, A., Poesen, J., Deckers, J., Kubik, P., 2007a. Restoring dense vegetation can slow mountain erosion to near natural benchmark levels. *Geology* 35, 303–306.
- Vanacker, V., Molina, A., Govers, G., Poesen, J., Deckers, J., 2007b. Spatial variation of suspended sediment concentrations in a tropical Andean river system: the Paute River, southern Ecuador. *Geomorphology* 87, 53–67.
- Wieczorek, G.F., 1987. Effect of rainfall intensity and duration on debris flows in Central Santa Cruz Mountains. In: Costa, J.E., Wieczorek, G.F. (Eds.), *Debris Flow/Avalanches: Process, Recognition, and Mitigation*. Geological Society of America: Reviews in Engineering Geology, 7, pp. 93–104 (Boulder, CO).
- Wilcke, W., Valladarez, H., Stoyan, R., Yasin, S., Valarezo, C., Zech, W., 2003. Soil properties on a chronosequence of landslides in montane rain forest, Ecuador. *Catena* 53, 79–95.